Ethylene Oligomerization and Polymerization by Palladium(II) Methyl Complexes Supported by Phosphines Bearing a Perchlorinated 10-Vertex *closo*-Carborane Anion Substituent

Jack F. Kleinsasser,[†,⊥] Erik D. Reinhart,[‡,⊥] Jess Estrada,[†] Richard F. Jordan,*[,‡] and Vincent Lavallo*[,†]

[†]Department of Chemistry, University of California Riverside, Riverside, CA 92521, United States

[‡]Department of Chemistry, The University of Chicago, 5735 South Ellis Avenue, Chicago, IL 60637, United States

ABSTRACT: The synthesis and ethylene reactivity of the zwitterionic Pd methyl complexes (κ^2-*P,Cl*-$PR_2CB_9Cl_9$)PdMe(THF) (**7**, R = ^{i}Pr; **8**, R = Ph) and (κ^2-*P,O*-P(*o*-OMe-Ph)$_2CB_9Cl_9$)PdMe(THF) (**9**), which contain the first phosphines appended with anionic 10-vertex perchlorinated *closo*-carboranes, are described. Complexes **7** and **8** oligomerize ethylene (23 °C, 2 atm) to a Schulz-Flory distribution of $C_4 - C_{10}$ olefins with TOFs of ca. 8000 and 1800 t.o./h respectively. **8** is ca. 4 times more active than the analogous (κ^2-*P,F,-ortho*-$PPh_2C_6H_4BF_3$)PdMe(L) (L = pyridine or collidine) system reported by Jordan and Piers, which produces butenes. Complex **9** reacts with ethylene to yield polyethylene wax (M_n ca. 1000, Đ ca. 1.5) that is similar to commercial Fisher-Tropsch waxes. The activities of **7**–**9** are independent of ethylene pressure and the presence of $B(C_6F_5)_3$, suggesting that the catalyst resting state is the corresponding ($PR_2CB_9Cl_9$)PdR(H_2C=CH_2) adduct. The molecular weights of the oligomer/polymer products are independent of ethylene pressure, which is consistent with an associative chain transfer mechanism. Reaction of **9** with ethylene generates the corresponding ethylene complex (κ^2-*P,O*-P(*o*-OMe-Ph)$_2CB_9Cl_9$)PdMe(H_2C=CH_2), which inserts ethylene at -20 ºC with a barrier ($\Delta G^{\neq}_{insertion}$) of 18.1 kcal/mol.

INTRODUCTION

Square planar palladium(II) alkyl complexes that contain unsymmetrical chelating phosphine-arenesulfonate ligands (**A**, Chart 1) have been studied extensively because of their ability to polymerize ethylene to linear polyethylene and copolymerize ethylene with polar monomers.[1–3] However, the performance of these catalysts is generally inferior compared to that of other classes of olefin polymerization catalysts, which has motivated studies of related catalysts with other unsymmetrical ligands.[4–12] One interesting analog of **A**, studied independently by the Jordan and Piers groups, is the zwitterionic phosphine-trifluoroborate system **B**, in which the sulfonate unit of **A** is replaced by a weakly-coordinating trifluoroborate group.[9,11] In the presence of ([$H(OEt_2)_2$][$B(3,5\text{-}(CF_3)_2\text{-}C_6H_3)_4$]) to sequester the collidine ligand as [collidinium][$B(3,5\text{-}(CF_3)_2\text{-}C_6H_3)_4$], **B** (L = collidine) catalytically dimerizes ethylene to butene with a turnover frequency (TOF) of 385 t.o./h at 23 °C (CD_2Cl_2 solvent, 150 psi ethylene). Under these conditions, the catalyst resting state is the (κ^2-*P,F-o*-$PPh_2C_6H_4BF_3$)PdEt(H_2C=CH_2) complex and the primary product 1-butene is isomerized to *cis* and *trans* 2-butene.

Carborane clusters offer interesting possibilities as frameworks or components for ligands for organometallic catalysts due to their structural rigidity, steric and electronic tunability[13–17] and synthetic availability.[18–30] In particular, halogenated *closo*-carborane anions are exceptionally stable[31,32] and may engage in weak dative BX→M interactions that may influence catalyst performance.[33]

Chart 1. Pd(II) Alkyl Complexes with Unsymmetrical Chelating Ligands. B atoms in the Carboranes are Represented as Unlabeled Vertices.

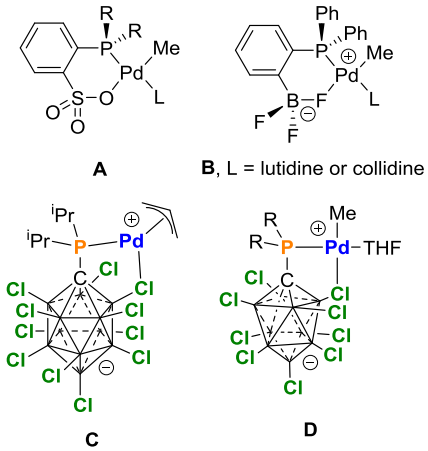

Lavallo and coworkers recently reported the synthesis and characterization of zwitterionic ($P^iPr_2CB_{11}Cl_{11}$)Pd(allyl) (**C**, Chart 1), bearing a diisopropyl phosphine ligand with a 12-vertex perchloro-*closo*-carborane anion substituent.[34] In the solid-state the $P^iPr_2CB_{11}Cl_{11}^-$ ligand in **C** is bound in an κ^2-*P,Cl* mode, and thus **C** may be viewed as a structural analogue

Scheme 1. Synthesis of Ligands and Complexes.

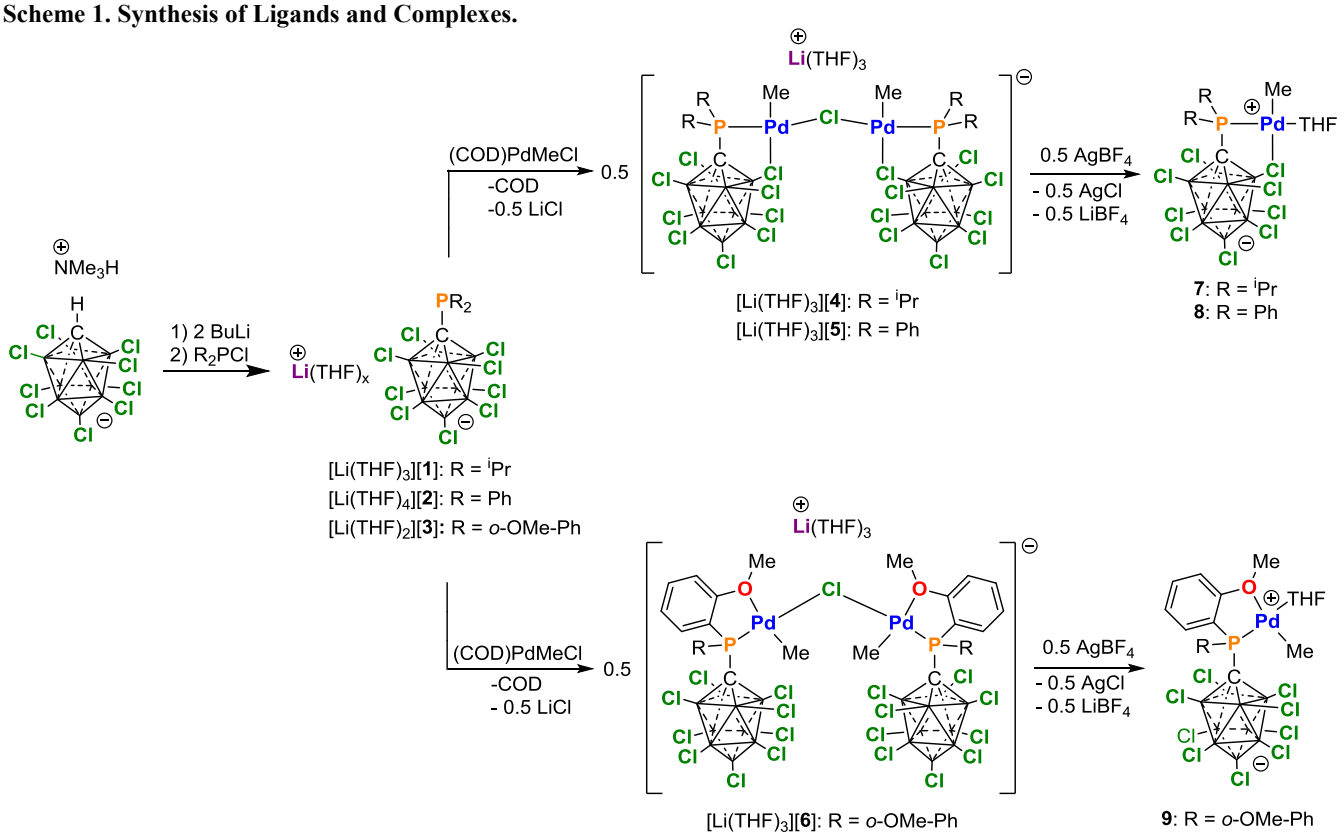

of **B**. Complex **C** reacts with norbornene to give organic-soluble polynorbornene but does not react with ethylene.

Here we describe the synthesis and reactivity with ethylene of $(PR_2CB_9Cl_9)PdMe(THF)$ complexes of type **D**, which contain phosphino-perchlorocarba-*closo*-decaborate ligands. Based on studies of the parent $P^iPr_2CB_9H_9^-$ and $P^iPr_2CB_{11}H_{11}^-$ ligands, a $PR_2CB_9Cl_9^-$ ligand is expected to be a stronger donor and to exhibit a slightly smaller cone angle compared to an analogous $PR_2CB_{11}Cl_{11}^-$ ligand.[14] The objective of the present work was to explore how these differences influence the reactivity of complexes of type **D** with ethylene. The steric and electronic properties of the phosphine-arenesulfonate ligands in **A** strongly influence the ethylene polymerization performance.[35] We report the synthesis of a new family of $PR_2CB_9Cl_9^-$ ligands (**1**, R = ^{i}Pr; **2**, R = Ph; **3**, R = *o*-OMe-Ph) and the corresponding zwitterionic $(PR_2CB_9Cl_9)PdMe(THF)$ complexes (**7**–**9**). Complexes **7** and **8**, which contain diisopropyl- and diphenyl-phosphino units respectively, are structurally analogous to **B**, with the $PR_2CB_9Cl_9^-$ ligands bound to Pd in a κ^2-*P,Cl* mode. In contrast, **9**, which contains a di-*o*-anisolyl phosphine unit, adopts a κ^2-*P,O* bonding mode in which one *o*-anisolyl methoxy group is bound to Pd.

RESULTS AND DISCUSSION

Synthesis and Characterization of $(PR_2CB_9Cl_9)PdMe(THF)$ Complexes. The $PR_2CB_9Cl_9^-$ ligands **1**–**3** were synthesized as the $Li(THF)_x$ salts (x = 2–4) following the procedure developed earlier for the 12-vertex analogue $[Li(THF)_3][P^iPr_2CB_{11}Cl_{11}]$ (Scheme 1).[19,34] C-Lithiation of $HCB_9Cl_9^-$ followed by addition of the appropriate

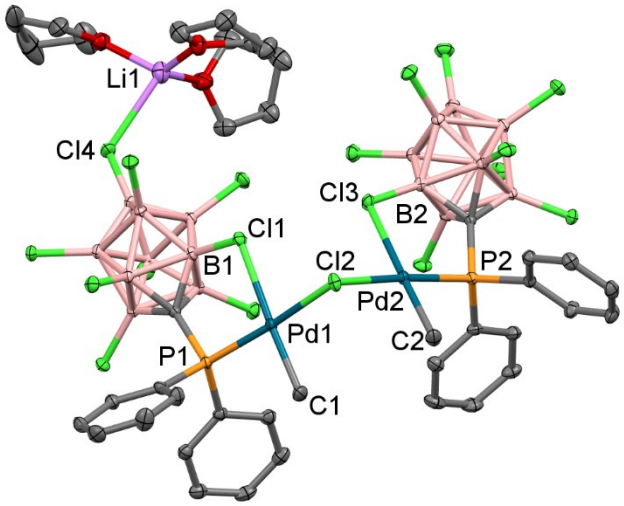

Figure 1. Solid state structure of $[Li(THF)_3][$**5**$]$: H atoms are omitted. Thermal ellipsoids are drawn at the 50% probability level. Key bond lengths (Å): Li1-Cl4 2.575(4) Pd1-C1 2.024(2), Pd1-P1 2.2255(6), Pd1-Cl1 2.4950(5), Pd1-Cl2 2.3847(6), B1-Cl1 1.790(2), Pd2-C2 2.024(2), Pd2-P2 2.2137(8), Pd2-Cl3 2.5600(5), Pd2-Cl2 2.3963(8), B2-Cl3 1.789(2). Key bond angles (º): C1-Pd1-P2 89.62(6), C1-Pd1-Cl2 84.70(2), P1-Pd1-Cl1 89.62(6), Cl2-Pd1-Cl 84.70(2), Pd1-Cl2-Pd2 103.34(2). Color code: C, gray; B, pink; Cl, green; P, orange; Pd, blue; O, red; Li, violet.

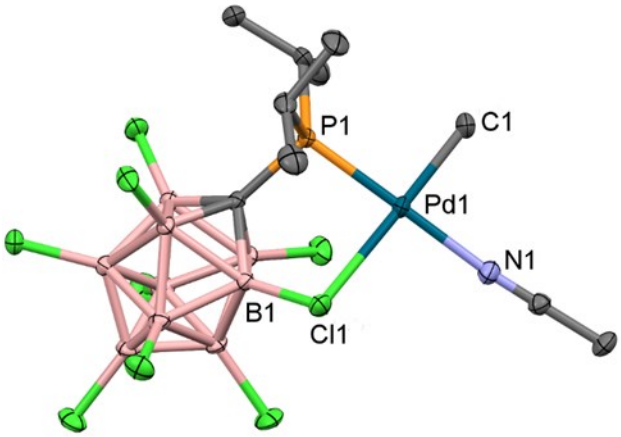

Figure 2. Solid state structure of **7–CH$_3$CN**•(PhF)$_{0.35}$. H atoms and PhF molecules are omitted and only one orientation of the disordered ^{i}Pr unit is shown. Thermal ellipsoids are drawn at the 50% probability level. Key bond lengths (Å): Pd1-C1 2.029(3), Pd1-P1 2.2329(6), Pd1-N1 2.088(2), Pd1-Cl1 2.5876(7), B1-Cl1 1.795(2). Key bond angles (º): C1-Pd1-P1 91.79(8), C1-Pd1-N1B 88.4(1), P1-Pd1-Cl1 87.36(2), N1-Pd1-Cl 92.78(6). Color code: C, gray; B, pink; Cl, green; P, orange; Pd, blue; O, red; N, light blue.

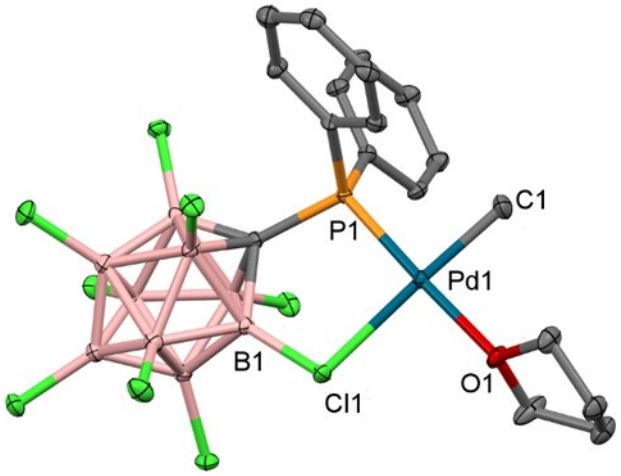

Figure 3. Solid state structure of **8**. H atoms are omitted. One orientation is shown. Thermal ellipsoids are drawn at the 50% probability level. Key bond lengths (Å): Pd1-C1 2.021(2), Pd1-O1 2.1362(15), Pd1-P1 2.2070(7), Pd1-Cl1 2.5135(6), B2-Cl1 1.800(2). Key bond angles (º): C1-Pd1-O1 90.05(8), C1-Pd1-P1 88.18(7), O1-Pd1-Cl1 88.71(5), Cl1-Pd1-P1 93.20(2). Color code: C, gray; B, pink; Cl, green; P, orange; Pd, blue; O, red.

R_2PCl electrophile affords [Li(THF)$_x$][**1**–**3**] in >90 % yield.

The reaction of [Li(THF)$_x$][**1**–**3**] with (COD)PdMeCl yields the chloro-bridged dinuclear complexes [Li(THF)$_3$][{($PR_2CB_9Cl_9$)PdMe}$_2$(μ-Cl)] ([Li(THF)$_3$][**4**]–[Li(THF)$_3$][**6**]). Reaction of [Li(THF)$_3$][**4**]–[Li(THF)$_3$][**6**] with 0.5 equiv of $AgBF_4$ yields the corresponding ($PR_2CB_9Cl_9$)PdMe(THF) complexes **7**–**9** in > 80% yield.

X-ray quality crystals of [Li(THF)$_3$][**5**] were grown from THF/pentane. Crystallization of **7** from CH_3CN/PhF gave X-ray quality crystals of the corresponding CH_3CN adduct ($P^iPr_2CB_9Cl_9$)PdMe(CH_3CN)•(PhF)$_{0.35}$ (**7–CH$_3$CN**•(PhF)$_{0.35}$). X-ray quality crystals of **8** were grown from PhF/hexanes. X-ray structural analyses of [Li(THF)$_3$][**5**], **7–CH$_3$CN**, and **8** (Figures 1–3) show that the $PR_2CB_9Cl_9^-$ ligands are bound in a κ^2-*P,Cl* mode in these complexes. The B–Cl bond lengths for the bound B–Cl units ([Li(THF)$_3$][**5**]: 1.790(2) Å , **7–CH$_3$CN**: 1.795(2) Å; **8**: 1.800(2) Å) are ca. 0.03 Å longer than average lengths of the terminal B–Cl bonds in the *ortho* layer of the carboranyl unit ([Li(THF)$_3$][**5**]: 1.761[1] Å , **7–CH$_3$CN**: 1.768[1] Å; **8**: 1.764[4] Å), similar to what is observed for **C**.[34] The 5-membered Pd–P–C–B–Cl chelate ring adopts an envelope conformation in **7** and a planar conformation in [Li(THF)$_3$][**5**] and **8**. The Pd-Me group is *cis* to phosphine in all three complexes as expected due to the stronger *trans* influence of the phosphine versus the weakly-coordinating B-Cl unit. In the solid-state structure of [Li(THF)$_3$][**5**], the positively charged $Li(THF)_3^+$ unit is in close contact with the sterically accessible *p*-Cl of one of the $CB_9Cl_9^-$ units, indicative of negative charge density on the these clusters.

X-ray quality crystals of **9**•(CH_2Cl_2)$_2$(pentane)$_{1.5}$ were grown from CH_2Cl_2/pentane. In contrast to the κ^2-*P,Cl* bonding mode observed for the $PR_2CB_9Cl_9^-$ ligands in [Li(THF)$_3$][**5**], **7–CH$_3$CN** and **8**, X-ray analysis shows that the P(*o*-OMe-Ph)$_2CB_9Cl_9^-$ ligand in **9** is bound in a κ^2-*P,O* mode through one of the *o*-anisolyl methoxy groups (Figure 4). The difference in structure between **8** and **9** may be driven by steric effects. Analysis of a space-filling model of **8** (Figures S59 and S60) reveals that the P*Ph$_2$* rings are pinned by the bulky perchlorocarboranyl unit in sterically crowded positions that would be inaccessible for the larger P*(o-OMe-Ph)$_2$* groups of **9**. Additionally, the ether functionality in **9** is a stronger donor compared to the weakly-coordinating B–Cl moiety of the $CB_9Cl_9^-$ unit. The Pd–P–C–C–O chelate ring in **9** adopts an envelope conformation. The non-Pd-bound –OMe group is positioned above the Pd square plane and is in close contact with the Pd center (Pd–O3 = 3.063 Å; sum of O and Pd van der Waals radii = 3.15 Å).

The $^{11}B\{^1H\}$ NMR spectra of [Li(THF)$_3$][**5**], **7**, and **8** contain three resonances in a 1:4:4 intensity ratio, indicative of effective C_{4v} symmetry of the $CB_9Cl_9^-$ cluster. This is consistent with the $CB_9Cl_9^-$ unit rotating rapidly around the C–P bond with concomitant exchange of the Pd-bound and non-Pd-bound B-Cl units on the *ortho*-ring of the carborane clusters in these compounds, as observed previously for **C**.[34]

The low temperature (-60 °C) ^1H NMR and $^{13}C\{^1H\}$ NMR spectra in CD_2Cl_2 of **9** contain two sets of *o*-anisolyl resonances (Figure 5). The difference in the chemical shifts of the –OMe resonances (^1H: Δδ = 0.32; ^{13}C: Δδ(^{13}C) = 3.7) is close to the coordination shift for the THF α-H resonances (^1H: $\delta_{bound} - \delta_{free}$ = 0.47; ^{13}C: $\delta_{bound} - \delta_{free}$ = 4.6), which is consistent with the coordination of one –OMe group to Pd, as observed in the solid-state structure. The ^1H NMR and $^{13}C\{^1H\}$ spectra of **9** in CD_2Cl_2 at room temperature contain one set of *o*-anisolyl resonances, indicating that the *o*-anisolyl groups exchange rapidly on the NMR timescale at this temperature (Figure 5). The barrier to anisolyl group exchange, $\Delta G^{\neq}$ = 12.3 kcal/mol, was determined from the coalescence of the –OMe ^1H NMR resonances ($T_{coalescence}$ = -5 °C, 500 MHz). The $^{11}B\{^1H\}$ NMR spectrum of **9** is similar to those of [Li(THF)$_3$][**5**], **7**, and **8**, indicat-

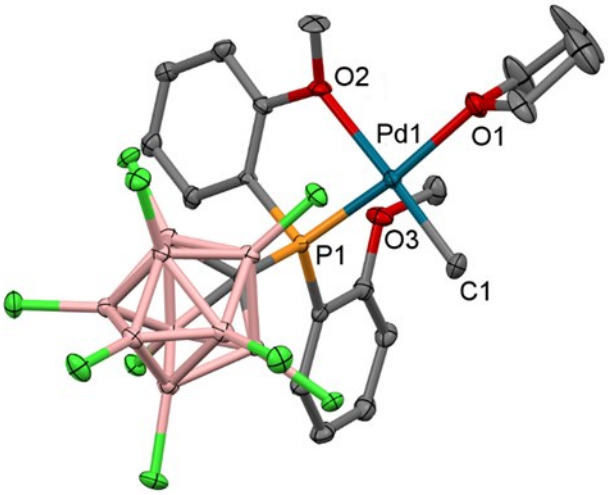

Figure 4. Solid state structure of **9**•$(CH_2Cl_2)_2$(pentane)$_{1.5}$. H atoms and CH_2Cl_2 and pentane solvent molecules are omitted. Thermal ellipsoids are drawn at the 50% probability level. Only one orientation of the disordered THF ligand is shown. Bond lengths (Å): Pd1-O1 2.127(1), Pd1-C1 2.019(1), Pd1-P1 2.1855(7), Pd1-O2 2.225(1). Key bond angles (º): O1-Pd1-C1 92.75(5), O1-Pd1-O2 89.98(4), C1-Pd1-P1 94.33(4), P1-Pd1-O1 82.53(3). Color code: C, gray; B, pink; Cl, green; P, orange; Pd, blue; O, red.

ing that the $CB_9Cl_9^-$ unit rotates rapidly around the C–P bond, regardless of the phosphine-carborane bonding mode, κ^2-*P,Cl* or κ^2-*P,O*.

The ^{1}H and ^{31}P{^{1}H} NMR spectra of [Li(THF)$_3$][**6**] at -60 ^{o}C in CD_2Cl_2 show that this species exists as a 1.6/1 mixture of two isomers, each of which exhibits two sets of anisolyl resonances in the ^{1}H spectrum. The isomers are assigned as diastereomers that differ in the relative configuration of the phosphorous atoms, which are stereogenic centers due to the κ^2-*P,O* bonding mode of the P(*o*-OMe-Ph)$_2$CB$_9$Cl$_9^-$ ligand. In contrast, only one species is observed at room temperature and -60 ºC in the ^{1}H and ^{31}P{^{1}H} NMR spectra of κ^2-*P,Cl*-[Li(THF)$_3$][**5**]. The difference in the ^{1}H chemical shifts for the Pd-bound and non-Pd-bound –OMe groups of [Li(THF)$_3$][**6**] ($\Delta\delta_{major\ isomer}$ = 0.52, $\Delta\delta_{minor\ isomer}$ = 0.80) of [Li(THF)$_3$][**6**] are similar to that for **9**. Isomer exchange is fast on the NMR time scale at 23 ºC due to fast exchange of the Pd-bound and non-Pd-bound methoxy groups.

Ethylene Reactivity. Complexes **7** and **8** oligomerize ethylene to a Schulz-Flory distribution of $C_4 - C_{10}$ olefins at 23 ºC and 2 atm ethylene pressure in mixed toluene/fluorobenzene solvent (Table 1). GC-MS analysis of the oligomers shows that **7** produces predominately α-olefins while **8** produces an approximately 1/1 mixture of α-olefins and internal olefins. Catalyst **7** is 5 times more active than **8**. In both cases, the catalytic activity and molecular weight distribution of the oligomers (as assessed by the Schulz-Flory propagation probability α, Figures S55 and S56)[36] are independent of ethylene pressure and are unaffected by the addition of B(C_6F_5)$_3$.

Complex **9** reacts with ethylene at 23 ^{o}C and 2 atm ethylene pressure to produce polyethylene (PE) wax with a narrow molecular weight distribution characteristic of a single-site catalyst (Table 2). At 50 ºC the activity is increased by a factor of 4 while the M_n value of the product is decreased by a factor of 3. As observed for **7** and **8**, the catalyst activity and M_n of the polymer are independent of ethylene pressure (up to 54 atm) and are unaffected by the presence of B(C_6F_5)$_3$.

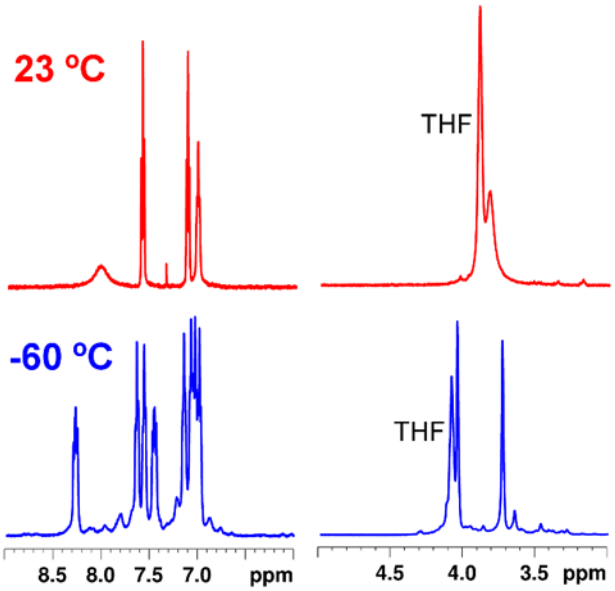

Figure 5. ^{1}H NMR spectra of **9** at 23 ºC (top) and -60 ºC (bottom) illustrating the exchange of the anisolyl rings. The aromatic and –OMe regions of the spectra are shown. The –OMe resonances appear at δ 4.05 and 3.73 at -60 ºC and are coalesced at 23 ºC (CD_2Cl_2).

The observation that the ethylene oligomerization/polymerization activity of **7**–**9** is independent of ethylene pressure and unaffected by the presence of B(C_6F_5)$_3$ suggests that the resting state for these catalysts is the corresponding ($PR_2CB_9Cl_9$)PdR'(CH_2=CH_2) ethylene complex (R' = growing chain). The observation that the molecular weight of the oligomer/polymer product is independent of ethylene pressure is consistent with an associative chain transfer mechanism, which is typical for square planar ethylene polymerization catalysts.[37]

Characterization of Polyethylene Produced by 9. The PE formed by **9** was characterized by ^{1}H and ^{13}C{^{1}H} NMR. Peak assignments were made based on literature data and 2D NMR experiments (see Supporting Information).[38–48] The PE produced by **9** at 23 ºC contains one olefin unit per chain, of which >95% are internal olefins. The internal olefins comprise primarily 2-olefins (42%), followed by 3-olefins (21%), 4-olefins (10%) and 5+-olefins (27%), with 70 % of the total olefins in the *trans* configuration. The PE produced at 50 ºC contains 90% internal olefins (Table 2, entry 2) in a 1/1 *cis*/*trans* ratio. The PEs produced at both 23 and 50 ºC contain ca. 13 branches per 1000 C (i.e. ca. one branch per chain) as determined by ^{1}H NMR. ^{13}C{^{1}H} NMR analysis shows that methyl, ethyl and *sec*-butyl branches are present in a 3/1/1 ratio. The PE microstructure is independent of ethylene pressure and is unaffected by the presence of B(C_6F_5)$_3$.

DSC analysis shows that the PE produced by **9** melts over a broad temperature range (Figure S71) with apparent T_m values

Table 1. Ethylene Oligomerization Data for Catalysts 7 and 8.[a]

Entry[b]	Cat.	P (atm)	Ethylene Consumed (mg)[d]	Activity (kg mol_{Pd}^{-1} h^{-1})	TOF (h^{-1})	α[e]	% α-olefin[f]
1	7[c]	2	420	210	7500	0.15	85
2	7[c]	6	470	240	8400	0.16	91
3[g]	7[c]	6	450	220	8000	0.17	83
4	8[h]	2	450	45	1600	0.22	47
5	8[h]	6	513	51	1800	0.17	46
6[g]	8[h]	6	540	54	1900	0.16	48

[a]Conditions: 49 mL toluene, 1 mL fluorobenzene, 23 ºC, 2 h. [b]Average of two identical runs. [c]1 μmol Pd. [d]Determined by mass flow. [e]Schulz-Flory propagation probability. [f]Percentage of olefins that are α-olefins, determined by GC-MS. [g]1 equiv of $B(C_6F_5)_3$ added. [h]5 μmol Pd.

Table 2. Ethylene Polymerization Data for Catalyst 9.[a]

Entry [b]	P (atm)	Yield (mg)	Activity (kg mol_{Pd}^{-1} h^{-1})	TOF (h^{-1})	M_n (Da)[c]	M_n (Da)[d]	Đ[d]	Branches /1000 C[c]	T_m (°C)[g]
1	2	103	10.3	370	1080	810	1.6	14	82.5, 92.3, 104.5
2[e]	2	345	34.5	1240	720	460	1.4	15	73.2, 89.2, 97.4
3	6	135	13.5	480	950	710	1.6	12	77.9,87.0, 103.0
4[f]	6	132	13.2	470	980	710	1.6	13	76.6, 86.6,102.6
5	54	100	10.0	360	810	580	1.5	14	71.0, 101.5

[a]Conditions: 49 mL toluene, 1 mL fluorobenzene, 23 ºC, 2 h, 5 μmol Pd. [b]Average of two identical runs. [c]Determined by ^{1}H NMR. [d]Determined by GPC. [e]50 ºC. [f]1 equiv of $B(C_6F_5)_3$ added. [g]Determined by DSC.

of ca. 80, 90, and 103 ºC (Table 2). Similar results have been observed for other low-molecular-weight PE waxes.[49–54] For example, saturated linear Fisher-Tropsch waxes, such as SasolWax H1 (M_n = 800, Đ = 1.4, 1.6 branches/1000 C), exhibit multiple melt transitions in DSC that are very similar to those observed for the PE formed by **9** (Figure S70). This behavior has been ascribed to the melting of crystallites consisting mainly of short chains at lower temperature and the progressive melting of crystallites composed primarily of longer and longer chains as the temperature is raised.[49,55–57]

Generation of a ($PR_2CB_9Cl_9$)PdMe(H_2C=CH_2) Ethylene Complex and Kinetics of PE Chain Growth. The reaction of **9** with ethylene was studied by NMR at low temperature in order to probe ethylene binding and monitor the chain growth process. The reaction of **9** with excess ethylene at -78 °C in CD_2Cl_2 generates the ethylene adduct (κ^2-*P,O*-P(*o*-OMe-Ph)$_2$$CB_9Cl_9$)PdMe($H_2C$=$CH_2$) (**10**, Scheme 2). The bound ethylene in **10** gives rise to an AA'BB' pattern at δ 5.42 and 5.30 in the ^{1}H NMR spectrum and a singlet at δ 101.5 in the $^{13}C\{^1H\}$ NMR spectrum at -78 °C, consistent with rapid rotation of the bound ethylene around the Pd-ethylene centroid bond.[58] The ^{1}H and $^{13}C\{^1H\}$ spectra of **10** at -78 °C contain two –OMe resonances, the chemical shift differences of which are similar to those observed for **9** and consistent with a κ^2-*P,O* bonding mode for the phosphine-carborane ligand. The Pd-Me group gives rise to a doublet in the ^{1}H NMR spectrum with a small $^3J_{PH}$ value (3 Hz) and a singlet in the $^{13}C\{^1H\}$ spectrum, indicating that the Me group is *cis* to the phosphine. The ^{1}H-^{1}H NOESY spectrum of **10** (-78 °C) contains strong correlations between the bound ethylene resonance and the Pd-Me resonance and one –OMe resonance (δ 4.03, Pd-bound), as well as a weak correlation with the other –OMe resonance at (δ 3.71, non-Pd-bound) (Figure S57). The bound ethylene ^{1}H NMR resonances are coalesced with the free ethylene resonance at -30 ºC. The –OMe ^{1}H NMR resonances are coalesced at -20 °C, indicating that **10** undergoes an anisolyl group ex-

Scheme 2. Generation of Ethylene Complex 10 and Subsequent Reaction with Ethylene to Generate 11.

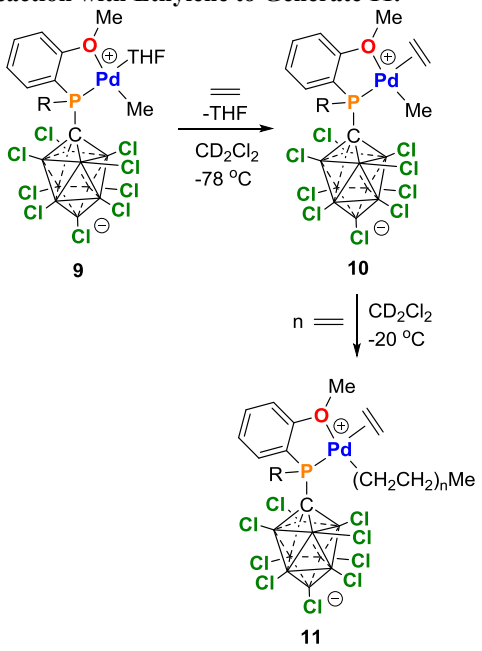

change process, as observed for **9**.

Complex **10** undergoes repetitive ethylene insertion at -20 °C to generate a mixture of (κ^2-*P,O*-P(*o*-OMe-Ph)$_2$CB$_9$Cl$_9$)PdR'(H$_2$C=CH$_2$) alkyl species (**11**, R' = growing chain). β–H elimination and olefin formation do not occur at this temperature and therefore the polymerization is living. The chain growth process was monitored by ^{1}H NMR. As 1 molecule of THF is released per equivalent of **9** in the formation of **10**, the total concentration of Pd species during chain growth is [Pd]$_{total}$ = [**10**] + [**11**] = [THF]. Therefore, the average number of ethylene units inserted per Pd-*R'* chain, X_n, is equal to the ratio (total integral of the Pd-*R'* resonances)/(integral of the THF β-H resonance).[59] Plots of X_n versus time are linear with a slope that is independent of ethylene concentration (Figure 6), indicating that the growth rate is zero-order in ethylene, which is consistent with the polymerization results. The composite insertion rate constant (for Pd-Me and Pd-R'), $k_{insertion}$ (eq 1), was determined to be 1.05(6) x 10^{-3} s^{-1} (-20 ºC), which corresponds to an apparent insertion barrier $\Delta G^{\neq}_{insertion}$ of 18.1(1) kcal/mol.

$$\frac{d(X_n)}{dt} = k_{insertion} \qquad (1)$$

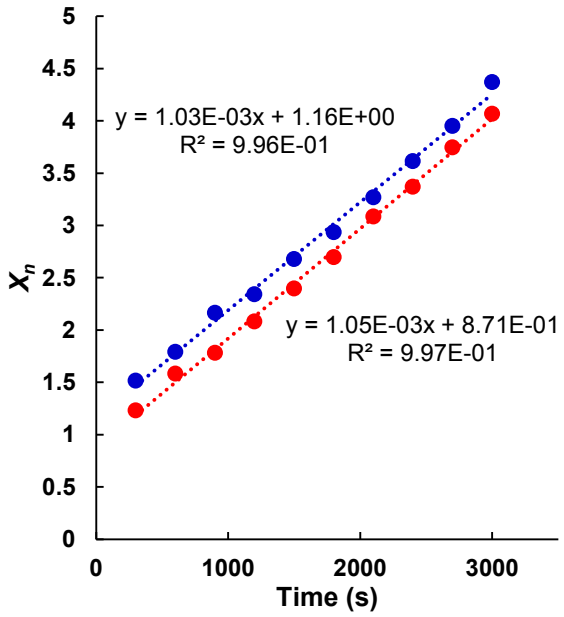

Figure 6. Representative plots of X_n versus time for the reaction of *in situ*-generated **10** with ethylene at -20 ºC. Blue data and curve: [Pd]$_{total}$ = 9.3 mM, [ethylene]$_{initial}$ = 0.15 M (16 equiv). Red data and curve: [Pd]$_{total}$ = 9.1 mM, [ethylene]$_{initial}$ = 0.32 M (35 equiv). The two curves do not overlap because the extent of chain growth at the beginning of data collection was different for the two runs. This difference affects the y intercept but not the slope of the line.

CONCLUSION

In conclusion, we have described the synthesis and characterization of **7**–**9**, which contain phosphino-perchlorocarba-*closo*-decaborate ligands. Compounds **7** and **8**, which contain κ^2-*P,Cl*-PR$_2$CB$_9$Cl$_9^-$ ligands, oligomerize ethylene to C$_4$-C$_{10}$ olefins, while **9**, which contains a κ^2-*P,O*-P(*o*-OMe-Ph)$_2$CB$_9$Cl$_9^-$ ligand, polymerizes ethylene to PE wax. These results contrast with the lack of reactivity with ethylene observed for PR$_2$CB$_{11}$Cl$_{11}^-$ complex **C**.[34] Catalyst **7**, which contains a strong donor P^{i}Pr$_2$ unit, is significantly more active than **8** or **9**, which contain P(aryl)$_2$ units. A similar trend was observed for analogous phosphine-arenesulfonate palladium alkyl catalysts **A**.[35] It is notable that **8** is ca. 4 times more reactive than the trifluoroborate analogue **B**/[H(OEt$_2$)$_2$][B(3,5-(CF$_3$)$_2$C$_6$H$_3$)$_4$], as assessed by the TOFs for ethylene oligomerization/dimerization.[9,11] As the catalyst resting state in both cases is the corresponding PdR(H$_2$C=CH$_2$) species, this reactivity trend is due to a difference in the ethylene insertion rate. The steric bulk of the perchlorocarborane backbone may contribute to the enhanced reactivity of **8**. The combination of the low molecular weight, low branch density, predominance of short branches, and preponderance of internal olefins in the polyethylene formed by **9** indicates that the secondary alkyl-metal species formed by chain walking undergo preferential chain transfer rather than chain growth.

EXPERIMENTAL SECTION

General Considerations. All manipulations were carried out using standard Schlenk or glovebox techniques under a nitrogen or argon atmosphere at room temperature unless otherwise stated. PhF was dried over and distilled from P_2O_5 or CaH_2. THF was dried and distilled from K metal. CH_2Cl_2, pentane, and toluene were purified by passage through BASF R3−11 oxygen scavenger and activated alumina. CD_2Cl_2 was dried over P_2O_5 or 3 Å molecular sieves and degassed. $CDCl_2CDCl_2$ and CD_3CN were dried over 3 Å molecular sieves and degassed. Unless specifically stated, reagents were purchased from commercial vendors and used without further purification. NMR spectra were recorded using Bruker Avance 300 MHz, Avance 400 MHz, Avance 500 MHz, or Avance 600 MHz instruments or a Varian Inova 300 MHz spectrometer. ^{1}H and ^{13}C NMR chemical shifts are reported relative to $SiMe_4$ and are internally referenced to the residual solvent resonance. ^{31}P NMR chemical shifts are externally referenced to H_3PO_4. ^{11}B NMR chemical shifts were externally referenced to BF_3Et_2O and the baseline of the spectra corrected using a multipoint spline. For all compounds, the carboranyl carbon resonance was not observed in ^{13}C{^{1}H} NMR spectra. NMR assignments for [Li(THF)$_3$][**1**]–**8** were made based on peak multiplicities and integrations. NMR assignments for **9** and **10** were made using 2D NMR experiments. High-resolution mass spectrometry (HRMS) was performed on an Agilent Technologies 6210 (TOF LC/MS) ESI/APCI instrument. [Me$_3$NH][HCB$_9$Cl$_9$] was synthesized according to literature procedures.[60] (COD)PdMeCl was synthesized according to literature procedures.[61] The purity of all isolated compounds was established by multinuclear NMR (see Supporting Information) and high resolution mass spectrometry.

[Li(THF)$_3$][P^{i}Pr$_2$CB$_9$Cl$_9$] ([Li(THF)$_3$][1]). [Me$_3$NH][HCB$_9$Cl$_9$] (0.500 g, 1.02 mmol) was dissolved in THF (3 mL) in a 20 mL scintillation vial equipped with a stir bar. *n*-BuLi (2.1 equiv, 2.0 M in hexanes) was added and the mixture was stirred for 30 min. This mixture was added to pentane (15 mL) that was being stirred and a white solid precipitated. The solid was collected by filtration, washed twice with pentane, and dried under vacuum. The resulting white powder was dissolved in THF (3 mL), ^{i}Pr$_2$PCl (171 mg, 1.12 mmol) was added, and the mixture was stirred for 1 h. The volatiles were removed under vacuum. The resulting oil was washed with pentane, taken up in PhF, and the insoluble LiCl was removed by filtration. The filtrate was

evaporated to dryness to yield [Li(THF)$_3$][**1**] as a white solid. Yield: 720 mg, 92%. ^{1}H NMR (400 MHz, CD_2Cl_2, 23 ºC): δ 3.79 (m, 12H, THF), 2.94 (d of septets, $^3J_{HH}$ = 7 Hz; $^2J_{PH}$ = 1.5 Hz, 2H), –C*H*(CH$_3$)$_2$), 1.98 (m, 12H, THF), 1.34 (two overlapping dds, $^3J_{PH}$ = 19 Hz, $^3J_{PH}$ = 11 Hz, $^3J_{HH}$ = 7.4 Hz, $^3J_{HH}$ = 6.9 Hz, 12H, –CH(C*H*$_3$)$_2$). ^{13}C{^{1}H} NMR (101 MHz, CD_2Cl_2, 23 ºC): δ 69.1 (THF), 25.9 (THF), 24.4 (d, $^2J_{PC}$ = 36 Hz, –CH(*C*H$_3$)$_2$), 22.2 (d, $^2J_{PC}$ = 26 Hz, –CH(*C*H$_3$)$_2$), 21.2 (d, $^1J_{PC}$ = 12 Hz, –*C*H(CH$_3$)$_2$). ^{11}B{^{1}H} NMR (96 MHz, CD_2Cl_2, 23 ºC): δ 23.6 (1B), -0.8 (4B), -2.4 (4B). ^{31}P{^{1}H} NMR (162 MHz, CD_2Cl_2, 23 ºC): δ 45.2. ESI/APCI HRMS (m/z): [M]$^-$ calculated for $C_7H_{14}B_9PCl_9$: 544.9044; found: 544.9044. mp: 100.0 – 106.7 ºC.

[Li(THF)$_4$][PPh$_2$CB$_9$Cl$_9$] ([Li(THF)$_4$][2]). [Li(THF)$_4$][**2**] was prepared from [Me$_3$NH][HCB$_9$Cl$_9$] (0.500 g, 1.02 mmol), *n*-BuLi (2.1 equiv, 2.0 M in hexanes) and Ph_2PCl (247 mg, 1.12 mmol) using the procedure described above for [Li(THF)$_3$][**1**]. Yield: white solid, 880 mg, 95%. ^{1}H NMR (300 MHz, CD_2Cl_2, 23 ºC): δ 8.07 (m, 4H, Ar), 7.37 (m, 6H, Ar), 3.78 (m, 16H, THF), 1.96 (m, 16H, THF). ^{13}C{^{1}H} NMR (101 MHz, CD_2Cl_2, 23 ºC): δ 137.5 (d, $^2J_{PC}$ = 29 Hz, *o*–Ph), 133.1 (d, $^1J_{PC}$ = 16 Hz, *ispo*–Ph), 130.1 (*p*–Ph), 128.0 (d, $^3J_{PC}$ = 10 Hz, *m*–Ph), 69.1 (THF), 25.9 (THF). ^{11}B{^{1}H} NMR (96 MHz, CD_2Cl_2, 23 ºC): δ 20.5 (1B), -4.3 (4B), -6.3 (4B). ^{31}P{^{1}H} NMR (162 MHz, CD_2Cl_2, 23 ºC): δ 11.5. ESI/APCI HRMS (m/z): [M]$^-$ calculated for $C_{13}H_{10}B_9PCl_9$: 612.8744; found: 612.8714. mp: 143.2 – 145.5 ºC.

[Li(THF)$_2$][P(*o*-Me-Ph)$_2$CB$_9$Cl$_9$] ([Li(THF)$_2$[3]). [Li(THF)$_2$[**3**] was prepared from [Me$_3$NH][HCB$_9$Cl$_9$] (0.500 g, 1.02 mmol), *n*-BuLi (2.1 equiv, 2.0 M in hexanes) and (*o*-OMe-Ph)$_2$PCl (315mg, 1.12 mmol) using the procedure described above for [Li(THF)$_3$][**1**]. Yield: white solid, 760 mg, 90%. ^{1}H NMR (400 MHz, CD_3CN, 23 ºC): δ 7.93 (m, 2H, Ar), 7.36 (m, 2H, Ar), 6.90 (m, 4H, Ar), 3.69 (s, 6H, -OC*H*$_3$), 3.65 (m, 8H, THF), 1.81 (m, 8H, THF). ^{13}C{^{1}H} NMR (101 MHz, CD_3CN, 23 ºC): δ 163.0 (d, $^2J_{PC}$ = 22 Hz, *C*–OCH$_3$), 137.7 (Ar), 131.9 (Ar), 123.2 (d, $^1J_{PC}$ = 29 Hz, *C*$_{ipso}$-P), 120.5 (Ar), 111.9 (Ar), 68.3 (THF), 56.4 (–O*C*H$_3$), 26.2 (THF). ^{11}B{^{1}H} NMR (96 MHz, CD_3CN, 23 ºC): δ 20.4 (1B), -4.4 (4B), -6.3 (4B). ^{31}P{^{1}H} NMR (162 MHz, CD_3CN, 23 ºC): δ -9.8. ESI/APCI HRMS (m/z): [M]$^-$ calculated for $C_{15}H_{14}B_9O_2PCl_9$: 672.9211; found: 672.9199. mp: 240.1 – 243.3 ºC.

(κ^2-*P,Cl*-P^{i}Pr$_2$CB$_9$Cl$_9$)PdMe(THF) (7). **1** (100 mg, 0.12 mmol) and PhF (1 mL) were added to a 20 mL scintillation vial equipped with a stir bar. (COD)PdMeCl (31.5 mg, 0.120 mmol) was separately dissolved in PhF (1 mL) in a second vial. The (COD)PdMeCl solution was slowly added to the solution of **1**. The second vial was washed with PhF (1 mL) and the wash was added to the solution of **1**. The mixture was stirred for 30 min and concentrated under vacuum. Pentane was added and the resulting light brown precipitate was allowed to settle. The pentane supernatant was decanted off and the precipitate was washed twice with pentane and dried under vacuum to yield [Li(THF)$_3$][**4**] as a brown solid. ^{1}H NMR (500 MHz, CD_2Cl_2, 23 ºC): δ 3.08 (m, 12 H, THF), 3.27 (m, 4H, –C*H*(CH$_3$)$_2$), 1.95 (m, 12H, THF), 1.73 (dd, $^3J_{HH}$ = 7.2 Hz, $^2J_{PH}$ = 19.0 Hz), 12 H, –CH(C*H*$_3$)$_2$), 1.01 (overlapping dd and s, $^3J_{HH}$ = 7.0 Hz, $^2J_{PH}$ = 17.5 Hz, 18H, Pd – C*H*$_3$ and –CH(C*H*$_3$)$_2$). ^{13}C{^{1}H} NMR (126 MHz, CD_2Cl_2, 23 ºC) δ 68.9 (THF), 27.0 ($^1J_{PC}$ = 20 Hz, -*C*H(CH$_3$)$_2$), 26.4 (THF), 23.0 (-CH(*C*H$_3$)$_2$), 19.9 (–CH(*C*H$_3$)$_2$), 0.3 (Pd –*C*H$_3$). ^{11}B{^{1}H} NMR (96 MHz, CD_3CN, 23 ºC): δ 24.0 (1B), -3.1 (4B), -5.6 (4B). ^{31}P{^{1}H} NMR (202 MHz, CD_2Cl_2, 23 ºC): δ 76.6. mp: 92.1 – 97.5 ºC (dec).

Without further purification, [Li(THF)$_3$][**4**] was dissolved in PhF (1mL) and $AgBF_4$ (11.0 mg, 0.0600 mmol) was added. The mixture was stirred for 30 min and filtered, and the collected solid was washed with CH_2Cl_2 (3 x 15 mL). The solvent was removed from the filtrate and washes under vacuum to afford **7** as a brown powder that contained a small amount of residual PhF. 81% pure by ^{31}P{^{1}H} NMR. Yield 77 mg, 87%. ^{1}H NMR (400 MHz, CD_2Cl_2, 23 ºC): δ 3.96 (m, 2H, THF), 3.28 (m, 2H, -C*H*(CH$_3$)$_2$), 1.97 (m, 2H, THF), 1.73 (dd, $^2J_{PH}$ = 20 Hz, $^3J_{HH}$ =7 Hz, 6H, –CH(C*H*$_3$)$_2$), 1.52 (dd, $^2J_{PH}$ = 20 Hz, $^3J_{HH}$ =7 Hz, 6H, –CH(C*H*$_3$)$_2$), 1.44 (s, 3H, Pd-C*H*$_3$). ^{13}C{^{1}H} NMR (101 MHz, CD_2Cl_2, 23 ºC): δ 72.9 (THF), 27.2 (d, $^2J_{PC}$ = 24 Hz, –CH(*C*H$_3$)$_2$), 25.6 (THF), 23.3 (br s, –CH(*C*H$_3$)$_2$), 20.0 (-*C*H(CH$_3$)$_2$), 1.2 (Pd-Me). ^{11}B{^{1}H} NMR (96 MHz, CD_2Cl_2, 23 ºC): δ 24.2 (1B), -3.4 (4B), -6.0 (4B). ^{31}P{^{1}H} NMR (162 MHz, CD_2Cl_2, 23 ºC): δ 77.5. ESI/APCI HRMS (m/z): [M – THF + CH_3CN]$^-$ calculated for $C_{10}H_{20}B_9NPCl_9Pd$: 701.8363; found: 701.8352. mp: 109.3 – 117.1 ºC (dec).

(κ^2-*P,Cl*-PPh$_2$CB$_9$Cl$_9$)PdMe(THF) (8). [Li(THF)$_3$][**5**] was generated as tan powder from **2** (100 mg, 0.110 mmol) and (COD)PdMeCl (28.9 mg, 0.110 mmol) using the procedure for [Li(THF)$_3$][**4**]. ^{1}H NMR (400 MHz, CD_2Cl_2, 23 ºC): δ 8.53 (dd, $^2J_{PH}$ = 12.5 Hz, $^3J_{HH}$ = 8.5 Hz, 8H, *o*–Ph), 7.60 (m, 12H, *m*–Ph and *p*–Ph), 3.78 (m, 12H, THF), 1.95 (m, 12H, THF), 1.38 (s, 6H, Pd–C*H*$_3$). ^{13}C{^{1}H} NMR: δ 138.5 (d, $^2J_{PC}$ = 16 Hz, *o*–Ph), 133.3 (d, $^4J_{PC}$ = 2 Hz, *p*–Ph), 128.8 (d, $^3J_{CP}$ = 12 Hz, *m*–Ph), 124.2 (d, $^1J_{CP}$ = 55 Hz, *ipso*–Ph), 69.2 (THF), 25.9 (THF), 12.6 (Pd–*C*H$_3$). ^{11}B{^{1}H} NMR (124 MHz, CD_2Cl_2, 23 ºC): δ 23.4 (1B), -3.16 (4B), -5.79 (4B). ^{31}P{^{1}H} NMR (162 MHz, CD_2Cl_2, 23 ºC): δ 56.6. Low temperature NMR data: ^{1}H NMR (500 MHz, CD_2Cl_2, -60 ºC): δ 8.48(dd, $^2J_{PH}$ = 12.5 Hz, $^3J_{HH}$ = 8.5 Hz, 8H, *o*-Ar), 7.59 (m, 12H, *m*-Ar and *p*-Ar), 3.66 (m, 16H, THF), 1.84 (m, 16H, THF), 1.30 (s, 6H, Pd-C*H*$_3$). ^{31}P{^{1}H} NMR (162 MHz, CD_2Cl_2, -60 ºC): δ 57.8. mp: 91.4 – 104.7 ºC (dec).

Without further purification, [Li(THF)$_3$][**5**] was reacted with $AgBF_4$ (10.7 mg, 0.06 mmol) using the procedure described above for **7** to yield **8** as a light brown powder. Yield: 78 mg, 88%. ^{1}H NMR (500 MHz, CD_2Cl_2, 23 ºC): δ 8.41 (dd, $^2J_{PH}$ = 12.5 Hz, $^3J_{HH}$ = 8.5 Hz, 4H, *o*–Ph), 7.63 (m, 6H, *m*–Ph and *p*–Ph), 4.09 (m, 4H, THF), 2.05 (m, 4H, THF), 1.18 (s, 3H, Pd–C*H*$_3$). ^{13}C{^{1}H} NMR (101 MHz, CD_2Cl_2, 23 ºC): δ 137.7 (d, $^2J_{PC}$ = 14 Hz, *o*-Ph), 133.7 (*p*-Ph), 129.0 (d, $^3J_{PC}$ = 13 Hz, *m*-Ph), 123.6 (d, $^1J_{PC}$ = 59 Hz, *ipso*-Ph), 71.2 (THF), 16.6 (THF), 14.6 (Pd-Me). ^{11}B{^{1}H} NMR (96 MHz, CD_2Cl_2, 23 ºC): δ 24.3 (1B), -3.2 (4B), -5.9 (4B). ^{31}P{^{1}H} NMR (162 MHz, CD_2Cl_2, 23 ºC): δ 56.6. ESI/APCI HRMS (m/z): [M – THF + CH_3CN]$^-$ calculated for $C_{16}H_{16}B_9NPCl_9Pd$: 779.8360; found: 779.8365. mp: 150.4 – 159.7 ºC (dec).

(κ^2-*P,O*-P(*o*-OMe-Ph)$_2$CB$_9$Cl$_9$)PdMe(THF) (9). [Li(THF)$_3$][**6**] was generated as a tan powder from **3** (100 mg, 0.10 mmol) and (COD)PdMeCl (27.3 mg, 0.100 mmol) using the procedure for [Li(THF)$_3$][**4**]. 94 % pure by inverse-gated ^{31}P{^{1}H} NMR. ^{1}H NMR (500 MHz, CD_2Cl_2, 23 ºC): δ 8.00 (br s, Ar, 3H, integration is lower than expected due to broadness), 7.54 (t, *J* = 7.7 Hz, 4H, Ar), 7.06 (t, *J* = 7.5 Hz, 4H, Ar), 6.99 (t, *J* = 7.1 Hz, 4H, Ar), 3.76 (overlapping m and br s, 24 H, –OC*H*$_3$ and THF), 1.94 (m, 12 H, THF), 1.13 (s, 6H, Pd-C*H*$_3$). ^{13}C{^{1}H} NMR (126 MHz, CD_2Cl_2, 23 ºC): δ 161.6 (br s, Ar), 136.1 (br s, Ar) 134.2 (Ar), 121.5 (br s, Ar), 112.6 (Ar), 69.0 (THF), 58.3 (br s, –O*C*H$_3$), 56.1 (br s, –O*C*H$_3$), 25.9 (THF), 0.7 (br s, Pd–*C*H$_3$). ^{11}B{^{1}H} NMR (96 MHz, CD_2Cl_2, 23 ºC): δ 24.2 (1B), -3.5 (4B), -6.0 (4B). Inverse-gated ^{31}P{^{1}H} NMR (162 MHz, CD_2Cl_2, 23 ºC): δ 21.2. Low temperature NMR data: Major isomer (62 %) ^{1}H NMR (500 MHz, CD_2Cl_2, -60 ºC): 4.08 (s, 6H –OC*H*$_3$,), 3.56 (s, 6H –OC*H*$_3$), 1.01 (s, 6H Pd–C*H*$_3$). ^{31}P{^{1}H} NMR (202 MHz, CD_2Cl_2, -60 ºC): 20.0. Minor isomer (38 %) ^{1}H NMR (500 MHz, CD_2Cl_2, -60 ºC): δ 4.18 (s, 6H, –OC*H*$_3$), 3.38 (s, 6H, –OC*H*$_3$), 0.97 (s, 6H, Pd–C*H*$_3$). Inverse-gated ^{31}P{^{1}H} NMR (202 MHz, CD_2Cl_2, -60 ºC): δ 20.4. The Ar resonances for these two species are overlapped. The ^{1}H NMR resonances for bound THF are observed at δ 3.66 and 1.83. mp: 125.3 – 129.8 ºC (dec).

Without further purification [Li(THF)$_3$][**6**] was reacted with $AgBF_4$ (10.0 mg, 0.0500 mmol) using the procedure described for **7** to yield **9** as a tan powder. Yield: 81 mg, 94% yield. The labelling scheme for **9** is shown in Figure 7. ^{1}H NMR (500 MHz, CD_2Cl_2, 23 ºC): δ 8.0 (br s, 2H, Ar), 7.59 (m, 2H, Ar), 7.12 (m, 2H, Ar), 7.01 (m, 2H, Ar), 4.04 (m, 4H, THF), 3.82 (br s, 6H, –OC*H*$_3$), 2.02 (m, 4H, THF), 0.89 (s,

3H, Pd–CH_3). $^{13}C\{^1H\}$ NMR (151 MHz, CD_2Cl_2, 23 ºC): δ 160.8 (*C*–OMe), 135.9 (br, Ar), 134.3 (br, Ar), 121.6 (br, Ar), 112.1 (Ar), 69.6 (THF), 57.8 (br s, –OCH_3), 25.4 (THF), 2.6 (br s, Pd–*C*H_3). $^{11}B\{^1H\}$ NMR (96 MHz, CD_2Cl_2, 23 ºC): δ 24.6 (1B), -4.0 (4B), -6.5 (4B). Inverse-gated $^{31}P\{^1H\}$ NMR (162 MHz, CD_2Cl_2, 23 ºC): δ 21.2. Low temperature NMR data[62]: ^1H NMR (500 MHz, CD_2Cl_2, -60 ºC): δ 8.27 (dd, $^3J_{PH}$ = 12.5 Hz, J_{HH} = 8 Hz, 1H, H^{13}), 7.64 (t, J_{HH} = 7.5 Hz ,1H, H^{11}), 7.56 (t, *J* = 7.5 Hz, H^4,), 7.45 (dd, $^3J_{PH}$ = 12.5 Hz, J_{HH} = 8 Hz, 1H, H^6), 7.14 (t, J_{HH} = 7 Hz, 1H, H^{12}), 7.08 (t, J_{HH} = $^4J_{PH}$ = 7.5 Hz, 1H, H^{10}), 7.04 (t, J_{HH} = 7.5 Hz, 1H, H^5), 6.98 (t, J_{HH} = $^4J_{PH}$ = 8 Hz , 1H, H^3), 4.09 (br m, 4H, THF), 4.05 (s, 3H, H^7), 3.73 (s, 3H, H^{14}), 2.01 (br m, 4H, THF), 0.71 (s, 3H, Pd-CH_3). $^{13}C\{^1H\}$ NMR (126 MHz, CD_2Cl_2, -60 ºC): δ 160.8 (d, $^2J_{PC}$ = 13 Hz, C^2), 158.8 (d, $^2J_{PC}$ = 9 Hz, C^9), 136.4 (C^{13}), 134.3 (C^{11}) 134.2 (C^4) 133.5 (C^{16}), 123.2 (C^5), 118.8 (d, $^2J_{PC}$ = 10 Hz, C^{12}), 115.5 (d, $^1J_{PC}$ = 58 Hz, C^1) 111.8 (d, $^2J_{PC}$ = 6 Hz, C^3), 111.1 (d, $^2J_{PC}$ = 8 Hz, C^{10}), 108.3 (d, $^1J_{PC}$ = 71 Hz, C^8) , 72.8 (THF), 59.6 (C^7), 55.9 (C^{14}), 25.1 (THF), 1.2 (Pd-CH_3). Inverse-gated $^{31}P\{^1H\}$ NMR (202 MHz, CD_2Cl_2, -60ºC): δ 20.8. HRMS: ESI/APCI HRMS (m/z): [M – THF + CH_3CN]$^-$ calculated for $C_{18}H_{20}B_9NO_2PCl_9Pd$: 829.8318; found: 829.8320. mp: 123.5 – 135.2 ºC (dec).

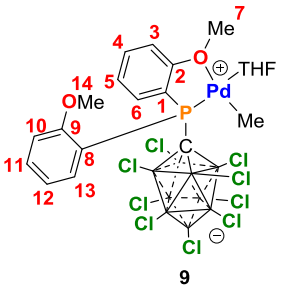

9

Figure 7. Numbering scheme for 9.

Generation of (κ^2-*P,O*-P(*o*-OMe-Ph)$_2$CB_9Cl_9)PdMe(CH_2=CH_2) (10). A solution of **9** (~5.0 mg) in CD_2Cl_2 was prepared in a J. Young NMR tube. The tube was cooled to -196 ºC in a liquid nitrogen bath and the desired amount of ethylene was added by vacuum transfer. The tube was allowed to thaw and warm to -78 ºC to afford a yellow-orange solution. The tube was shaken several times to ensure proper mixing of ethylene into the solvent and then was placed in an NMR probe that had been precooled to -78 ºC.[62] The numbering scheme for **10** is shown in Figure 8. ^1H NMR (CD_2Cl_2, 500 MHz, -78 ºC): δ 8.30 (dd, J_{HH} =8 Hz, J_{PH} = 12 Hz, 1H, H^{13}), 7.66 (t, *J* = 8 Hz, 1H, H^{11}), 7.57 (t, *J*=7.5 Hz, 1H, H^4), 7.43 (dd, J_{HH} =8 Hz, J_{PH} = 12 Hz, 1H, H^6), 7.18 (t, *J* =7 Hz, 1H, H^{12}), 7.05 (t, *J* =7.5 Hz, 2H, H^3 and H^5), 6.99 (dd, J_{HH} =8 Hz, J_{PH} = 8 Hz, H^{10}), 5.42 (br d, *J* = 9 Hz, 2H, bound ethylene AA'), 5.36 (s, free ethylene), 5.30 (br d, bound ethylene BB' (overlapped with solvent resonance)), 4.03 (s, 3H, H^7), 3.71 (s, 3H, H^{14}), 3.61 (m, 4H, free THF), 1.74 (m, 4H, free THF), 0.82 (s, $^3J_{PH}$ = 3 Hz, 3H, Pd-CH_3). $^{13}C\{^1H\}$ NMR (CD_2Cl_2, 126 MHz, -78 ºC): δ 161.3 (d, $^2J_{PC}$ = 15 Hz, C^9), 158.2 (d, $^2J_{PC}$ = 10 Hz, C^2), 136.8 (C^{13}), 134.5 (C^1), 134.1 (C^4), 134.0 (C^{11}), 123.6 (C^5), 122.8 (s, free ethylene), 119.1 (C^{12}), 114.7 (d, $^1J_{PC}$ = 54 Hz, C^1), 112.0 (C^3), 111.4 (C^{10}), 107.0 (d, $^1J_{PC}$ = 61 Hz, C^8), 101.5 (s, bound ethylene), 67.3 (s, free THF), 60.4 (C^7), 56.0 (C^{14}), 25.0 (free THF), 5.9 (Pd-CH_3). Inverse-gated $^{31}P\{^1H\}$ NMR (202 MHz, CD_2Cl_2, -78 ºC): δ 9.8.

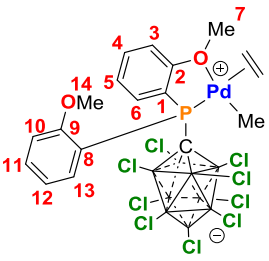

10

Figure 8. Numbering scheme for 10.

Chain Growth of 10 at -20 ºC. A solution of **10** in CD_2Cl_2 containing excess ethylene (16, 26, or 35 equiv) was generated in a J. Young NMR tube as described above. The tube was placed in the NMR probe that was prechilled to -25 ºC and equilibrated for 10 min. The probe was then warmed to -20 ºC and the tube was monitored by ^1H NMR for ca. 1 h. The resonances for **10** disappeared and resonances assigned to **11** higher alkyl species grew in. Key ^1H NMR data for **11**: δ 4.02 (s, –OCH_3), 3.56 (s, –OCH_3), 2.40 (br s), 2.23 (br s), 1.99 (br s), 1.22 (s, –CH_2–), 1.16 (br m), 0.97 (br m), 0.83 (q, J_{HH} = 7 Hz), 0.78 (t, J_{HH} = 8 Hz, –CH_3), 0.65 (t, J_{HH} =7 Hz, –CH_3), 0.59 (t, J_{HH} = 8 Hz, –CH_3).

Low pressure ethylene oligomerization and polymerization reactions. Ethylene oligomerization/polymerization reactions at 2 and 6 atm were performed in a 200 mL Fischer-Porter bottle equipped with a 2-inch long Teflon-coated magnetic stir bar and a stainless-steel pressure head fitted with inlet and outlet needle valves, a septum-capped ball valve for injections, a safety check valve, and a pressure gauge. In a N_2-filled glovebox, the Fischer-Porter bottle was charged with toluene (49 mL). The apparatus was removed from the glovebox, connected to a stainless-steel double manifold vacuum/ethylene line, placed in a room temperature water bath or 50 ºC oil bath, and stirred at 370 rpm. The N_2 atmosphere was replaced with ethylene by three evacuation-refill cycles. The solution was equilibrated at either 2 or 6 atm of ethylene pressure for 15 min. For the 2 atm experiments, a freshly-prepared stock solution of catalyst in PhF (1 mL) was added via gas-tight syringe. For the 6 bar experiments, the pressure was decreased to 1.4 atm, a stock solution of catalyst in PhF (1 mL) was added immediately via gas-tight syringe, and the pressure was immediately increased to 6 atm. The ethylene pressure was kept constant by feeding ethylene on demand.

For catalysts **7** and **8**, ethylene consumption was measured using a Brooks Instruments 5860i Mass Flow Sensor. The total ethylene consumption was determined by numerical integration of the mass flow curve using the LabView software package. Control experiments showed that equilibration of ethylene between the gas and solution phases at 6 atm ethylene pressure requires ca. 15 min under the reaction conditions (23 ºC, 370 rpm stirring), and therefore the activity for the 6 atm experiments was determined using the mass flow curve excluding the first 15 min. After 2 h, the ethylene line was closed, the Fischer-Porter bottle was vented, *o*-xylene (100 μL) was added as an internal standard, and the solution was analyzed by GC-MS using an Aglient 6890/5973N GC-MS instrument. The masses of hexene, octene, and decene were determined by GC-MS using predetermined response factors. The mass of butene was calculated by subtracting the masses of the other oligomers from the total mass of ethylene consumed.

For catalyst **9**, after the ethylene line was closed and the Fisher-Porter bottle was vented, methanol (50 mL) was added to precipitate the polymer. The polymer was collected by filtration, washed with methanol (50 mL), and dried for 2 d at 70 ºC in a vacuum oven.

High pressure ethylene polymerization reactions. Ethylene polymerizations at 54 atm were performed using a stainless-steel Parr 300 mL autoclave, which was equipped with a magnetically-driven

1.5-inch diameter four-blade propeller stirrer, thermocouple, water cooling loop, and a Parr 4842 controller. In a N_2 glovebox, a 200 mL glass autoclave liner was charged with toluene (49 mL) and a stock solution of the catalyst in PhF (1 mL) and placed in the autoclave. The autoclave was sealed, removed from the glovebox, and attached to the ethylene line. The mixture was stirred (270 rpm) at 23ºC for 15 min and then pressurized to 54 atm of ethylene. The ethylene pressure was kept constant by feeding ethylene on demand. After 2 h the ethylene line was closed and the autoclave was vented. Methanol (50 mL) was added to precipitate the polymer, which was characterized as described above.

DSC measurements were performed on a TA Instruments 2920 differential scanning calorimeter. Samples (5 mg) were annealed by heating to 170 ºC at 15 C/min, cooled to 0 ºC at 10 °C/min, and analyzed by heating to 170 °C at 15 °C/min. ^{1}H and ^{13}C{^{1}H} NMR spectra of PE samples were obtained at 100 ºC in dry degassed $CDCl_2CDCl_2$ solvent using a Bruker Advance 500 NMR instrument. Gel permeation chromatography (GPC) was performed on a Polymer Laboratories PL−GPC 200 instrument at 150 °C with 1,2,4-trichlorobenzene (stabilized with 125 ppm BHT) as the mobile phase. Three PLgel 10 μm Mixed-B LS columns were used. The molecular weights were calibrated using narrow polystyrene standards with a 10-point calibration of M_n from 570 Da to 5670 kDa, and are corrected for linear polyethylene by universal calibration by using the following Mark−Houwink parameters: polystyrene, $K = 1.75 \times 10{-}2$ cm^3 g^{-1} , $\alpha = 0.67$; polyethylene, $K = 5.90 \times 10^{-2}$ cm^3 g^{-1} , $\alpha = 0.69$.[63]

ASSOCIATED CONTENT

Supporting Information

The Supporting Information is available free of charge on the ACS Publications website.

NMR spectra for compounds and polyethylene formed by **9**, and supporting figures (PDF)

Accession Codes

CCDC 1871350 ([Li(THF)$_3$][**5**]), 1867545 (**7**), 1867546 (**8**), 1867547 (**9**) contain the supplementary crystallographic data for this paper. These data can be obtained free of charge via www.ccdc.cam.ac.uk/data_request/cif, or by emailing data_request@ccdc.cam.ac.uk, or by contacting The Cambridge Crystallographic Data Centre, 12, Union Road, Cambridge CB2 1EZ, UK; fax: +44 1223 336033.

AUTHOR INFORMATION

Corresponding Authors

*R.F.J: email, rfjordan@uchicago.edu
*V.L.: email, vincent.lavallo@ucr.edu

Author Contributions

⊥These authors contributed equally to this work.

ORCID

Jack Kleinsasser: 0000-0003-3910-1717
Erik D. Reinhart: 0000-0003-2878-9376
Richard F. Jordan: 0000-0002-3158-4745
Vince Lavallo: 0000-0001-8945-3038

Notes

The authors declare no competing financial interest.

ACKNOWLEDGMENT

This work was supported by the National Science Foundation (NSF) under grant number CHE-1709159 and CHE-1455348. NMR studies were also partially supported by NSF MRI grant CHE-1626673. We thank Dr. Antoni Jurkiewicz and Dr. Dan Borchardt for assistance with NMR, Dr. Alexander Filatov, Dr. Fook S. Tham and Andrew McNeece for X-ray crystallography, and Dr. Zie Zhou for mass spectrometry.

REFERENCES

(1) Nakamura, A.; Anselment, T. M. J.; Claverie, J.; Goodall, B.; Jordan, R. F.; Mecking, S.; Rieger, B.; Sen, A.; van Leeuwen, P. W. N. M.; Nozaki, K. Ortho-phosphinobenzenesulfonate: a Superb Ligand for Palladium-catalyzed Coordination-insertion Copolymerization of Polar Vinyl Monomers. *Acc. Chem. Res.* **2013**, *46*, 1438–1449.

(2) Ito, S.; Nozaki, K. Coordination-insertion Copolymerization of Polar Vinyl Monomers by Palladium Catalysts. *Chem. Rec.* **2010**, *10*, 315–325.

(3) Nakamura, A.; Ito, S.; Nozaki, K. Coordination-insertion Copolymerization of Fundamental Polar Monomers. *Chem. Rev.* **2009**, *109*, 5215–5244.

(4) Sui, X.; Dai, S.; Chen, C. Ethylene Polymerization and Copolymerization with Polar Monomers by Cationic Phosphine Phosphonic Amide Palladium Complexes. *ACS Catal.* **2015**, *5*, 5932–5937.

(5) Zhang, Y.; Cao, Y.; Leng, X.; Chen, C.; Huang, Z. Cationic Palladium(II) Complexes of Phosphine–Sulfonamide Ligands: Synthesis, Characterization, and Catalytic Ethylene Oligomerization. *Organometallics* **2014**, *33*, 3738–3745.

(6) Mitsushige, Y.; Carrow, B. P.; Ito, S.; Nozaki, K. Ligand-controlled Insertion Regioselectivity Accelerates Copolymerisation of Ethylene with Methyl Acrylate by Cationic Bisphosphine Monoxide–palladium Catalysts. *Chem. Sci.* **2016**, *7*, 737–744.

(7) Noda, S.; Nakamura, A.; Kochi, T.; Chung, L. W.; Morokuma, K.; Nozaki, K. Mechanistic Studies on the Formation of Linear Polyethylene Chain Catalyzed by Palladium Phosphine-sulfonate Complexes: Experiment and Theoretical Studies. *J. Am. Chem. Soc.* **2009**, *131*, 14088–14100.

(8) Contrella, N. D.; Sampson, J. R.; Jordan, R. F. Copolymerization of Ethylene and Methyl Acrylate by Cationic Palladium Catalysts That Contain Phosphine-Diethyl Phosphonate Ancillary Ligands. *Organometallics* **2014**, *33*, 3546–3555.

(9) Kim, Y.; Jordan, R. F. Synthesis, Structures, and Ethylene Dimerization Reactivity of Palladium Alkyl Complexes That Contain a Chelating Phosphine–trifluoroborate Ligand. *Organometallics* **2011**, *30*, 4250–4256.

(10) Johnson, A. M.; Contrella, N. D.; Sampson, J. R.; Zheng, M.; Jordan, R. F. Allosteric Effects in Ethylene Polymerization Catalysis. Enhancement of Performance of Phosphine-Phosphinate and Phosphine-Phosphonate Palladium Alkyl Catalysts by Remote Binding of $B(C_6F_5)_3$. *Organometallics* **2017**, *36*, 4990–5002.

(11) Gott, A. L.; Piers, W. E.; Dutton, J. L.; McDonald, R.; Parvez, M. Dimerization of Ethylene by Palladium Complexes Containing Bidentate Trifluoroborate-Functionalized Phosphine Ligands. *Organometallics* **2011**, *30*, 4236–4249.

(12) Wucher, P.; Goldbach, V.; Mecking, S. Electronic Influences in Phosphinesulfonato palladium(II) Polymerization Catalysts. *Organometallics* **2013**, *32*, 4516–4522.

(13) Spokoyny, A. M.; Lewis, C. D.; Teverovskiy, G.; Buchwald, S. L. Extremely Electron-Rich, Boron-Functionalized, Icosahedral Carborane-Based Phosphinoboranes. *Organometallics* **2012**, *31*, 8478–8481.

(14) Estrada, J.; Lugo, C. A.; McArthur, S. G.; Lavallo, V. Inductive Effects of 10 and 12-vertex *closo*-carborane Anions: Cluster Size and Charge Make a Difference. *Chem. Commun.* **2016**, *52*, 1824–1826.

(15) Fisher, S. P.; El-Hellani, A.; Tham, F. S.; Lavallo, V. Anionic and Zwitterionic Carboranyl N-heterocyclic Carbene Au(I) Complexes. *Dalton Trans.* **2016**, *45*, 9762–9765.

(16) Riley, L. E.; Krämer, T.; McMullin, C. L.; Ellis, D.; Rosair, G. M.; Sivaev, I. B.; Welch, A. J. Large, Weakly Basic Bis(carboranyl)phosphines: An Experimental and Computational Study. *Dalton Trans.* **2017**, *46*, 5218–5228.

(17) King, A. S.; Ferguson, G.; Britten, J. F.; Valliant, J. F. Sterically Hindered and Robust Pnictogen Ligands Derived from Carboranes: Synthesis and X-ray Structure Determination of Tris(1'-methyl(1,2-dicarba-*closo*-dodecaboran-1-yl))phosphine, Tris(1'-methyl(1,2-dicarba-*closo*-dodecaboran-1-yl))arsine and chloro(tris(1'-methyl(1,2-dicarba-*closo*-dodecaboran-1-yl))phosphine)gold(I). *Inorg. Chem.* **2004**, *43*, 3507–3513.

(18) Soloway, A. H.; Tjarks, W.; Barnum, B. A.; Rong, F.-G.; Barth, R. F.; Codogni, I. M.; Wilson, J. G. The Chemistry of Neutron Capture Therapy. *Chem. Rev.* **1998**, *98*, 1515–1562.

(19) Lavallo, V.; Wright, J. H.; Tham, F. S.; Quinlivan, S. Perhalogenated Carba-*closo*-dodecaborate Anions as Ligand Substituents: Applications in Gold Catalysis. *Angew. Chem. Int. Ed. Engl.* **2013**, *52*, 3172–3176.

(20) Spokoyny, A. M. New Ligand Platforms Featuring Boron-rich Clusters as Organomimetic Substituents. *Pure Appl. Chem.* **2013**, *85*.

(21) Olid, D.; Núñez, R.; Viñas, C.; Teixidor, F. Methods to Produce B-C, B-P, B-N and B-S Bonds in Boron Clusters. *Chem. Soc. Rev.* **2013**, *42*, 3318–3336.

(22) Douvris, C.; Michl, J. Update 1 of: Chemistry of the Carba-*closo*-dodecaborate(-) Anion, $CB_{11}H_{12}^-$. *Chem. Rev.* **2013**, *113*, PR179–233.

(23) Popescu, A. R.; Teixidor, F.; Viñas, C. Metal Promoted Charge and Hapticities of Phosphines: The Uniqueness of Carboranylphosphines. *Coord Chem Rev* **2014**, *269*, 54–84.

(24) Scholz, M.; Hey-Hawkins, E. Carbaboranes as Pharmacophores: Properties, Synthesis, and Application Strategies. *Chem. Rev.* **2011**, *111*, 7035–7062.

(25) Grimes, R. N. Carboranes in the Chemist's Toolbox. *Dalton Trans.* **2015**, *44*, 5939–5956.

(26) Xie, Z. Cyclopentadienyl-carboranyl Hybrid Compounds: a New Class of Versatile Ligands for Organometallic Chemistry. *Acc. Chem. Res.* **2003**, *36*, 1–9.

(27) Yao, Z.-J.; Jin, G.-X. Transition Metal Complexes Based on Carboranyl Ligands Containing N, P, and S Donors: Synthesis, Reactivity and Applications. *Coord Chem Rev* **2013**, *257*, 2522–2535.

(28) (a) *Boron Science: New Technologies and Applications*; Hosmane, N., Ed.; 1st ed.; CRC Press: Boca, Raton, Florida, 2011. (b) Hosmane, N. S. *Handbook of Boron Chemistry in Organometallics, Catalysis, Materials and Medicine*; Eagling, R., Ed.; 1st ed.; Imperial College Press/World Scientific Publishing: London, 2018.

(29) Grimes, R. N. *Carboranes*; 3rd ed.; Elsevier: London, 2016.

(30) (a) Dodge, T.; Curtis, M. A.; Russell, J. M.; Sabat, M.; Finn, M. G.; Grimes, R. N. Titanium and Zirconium $Et_2C_2B_4H_4$ −metal−phosphine Complexes: Synthesis, Characterization, and Ethylene Polymerization Activity. *J. Am. Chem. Soc.* **2000**, *122*, 10573–10580. (b) Boring, E.; Sabat, M.; Finn, M. G.; Grimes, R. N. Alkene and Alkyne Insertion Reactions with Tantalum Metallacarborane Complexes: the $Et_2C_2B_4H_4^{2-}$ Carborane Ligand as a Spectator and Participant. *Organometallics* **1998**, *17*, 3865–3874. (c) Boring, E.; Sabat, M.; Finn, M. G.; Grimes, R. N. Alkene and Alkyne Insertion Reactions with Tantalum Metallacarborane Complexes: the $Et_2C_2B_4H_4^{2-}$ Carborane Ligand as a Spectator and Participant. *Organometallics* **1998**, *17*, 3865–3874. (d) Yinghuai, Z.; Hosmane, N. S. Carborane-based Transition Metal Complexes and Their Catalytic Applications For Olefin Polymerization: Current and Future Perspectives. *J. Organomet. Chem.* **2013**, *747*, 25–29. (e) Yinghuai, Z.; Nong, L. C.; Zhao, L. C.; Widjaja, E.; Hwei, C. S.; Cun, W.; Tan, J.; Meurs, M. V.; Hosmane, N. S.; Maguire, J. A. Synthesis, Characterization, and Polymerization of a Neutral Tantalacarborane Sandwich Complex Derived from a Pentaanionic Exo-Polyhedrally Linked Bis(C_2B_{10}-carborane) Ligand. *Organometallics* **2009**, *28*, 60–64. (f) Yinghuai, Z.; Yulin, Z.; Carpenter, K.; Maguire, J. A.; Hosmane, N. S. Syntheses and Catalytic Activities of Group 4 Metal Complexes Derived from C(cage)-appended Cyclohexyloxocarborane Trianion. *J. Organomet. Chem.* **2005**, *690*, 2802–2808. (g) Paxson, T. E.; Hawthorne, M. F. Preparation of Hydridometallocarboranes and Their Use as Homogeneous Catalysts. *J. Am. Chem. Soc.* **1974**, *96*, 4674–4676. (h) Hewes, J. D.; Kreimendahl, C. W.; Marder, T. B.; Hawthorne, M. F. Metal-promoted Insertion of an Activated Alkene into a Boron-hydrogen Bond of an Exopolyhedral *nido*-rhodacarborane: Rhodium-catalyzed Hydroboration. *J. Am. Chem. Soc.* **1984**, *106*, 5757–5759. (i) Long, J. A.; Marder, T. B.; Behnken, P. E.; Hawthorne, M. F. Metallacarboranes in Catalysis. 3. Synthesis and Reactivity of exo-*nido*-phosphinerhodacarboranes. *J. Am. Chem. Soc.* **1984**, *106*, 2979–2989. (j) Zhu, Y.; Carpenter, K.; Ching, C. B.; Bahnmueller, S.; Chan, P. K.; Srid, V. S.; Leong, W. K.; Hawthorne, M. F. (R)-BINAP-mediated Asymmetric Hydrogenation with a Rhodacarborane Catalyst in Ionic-liquid Media. *Angew. Chem. Int. Ed. Engl.* **2003**, *42*, 3792–3795. (k) Behnken, P. E.; Busby, D. C.; Delaney, M. S.; King, R. E.; Kreimendahl, C. W.; Marder, T. B.; Wilczynski, J. J.; Hawthorne, M. F. Metallacarboranes in Catalysis. Kinetics and Mechanism of Acrylate Ester Hydrogenation Catalyzed by *closo*-rhodacarboranes. *J. Am. Chem. Soc.* **1984**, *106*, 7444–7450. (l) Crowther, D. J.; Baenziger, N. C.; Jordan, R. F. Group 4 Metal Dicarbollide Chemistry. Synthesis, Structures, and Reactivity of Electrophilic Alkyl Complexes (Cp*)($C_2B_9H_{11}$)M(R), M = Hf, Zr. *J. Am. Chem. Soc.* **1991**, *113*, 1455–1457. (m) Kreuder, C.; Jordan, R. F.; Zhang, H. Early Metal Carborane Chemistry. Generation and Reactivity of (C_5Me_5)(η^5-$C_2B_9H_{11}$)TiMe. *Organometallics* **1995**, *14*, 2993–3001. (n) Yoshida, M.; Jordan, R. F. Catalytic Dimerization of Terminal Alkynes by a Hafnium Carboranyl Complex. A "Self-Correcting" Catalyst. *Organometallics* **1997**, *16*, 4508–4510.

(31) Reed, C. A. Carborane Acids. New "Strong yet Gentle" Acids for Organic and Inorganic Chemistry. *Chem. Commun.* **2005**, 1669–1677.

(32) Reed, C. A. Carboranes: A New Class of Weakly Coordinating Anions for Strong Electrophiles, Oxidants, and Superacids. *Acc. Chem. Res.* **1998**, *31*, 133–139.

(33) Grimes, R. N. Carboranes in Catalysis. *Carboranes*; 3rd ed.; Elsevier: London, 2016; pp. 929–944.

(34) Estrada, J.; Woen, D. H.; Tham, F. S.; Miyake, G. M.; Lavallo, V. Synthesis and Reactivity of a Zwitterionic Palladium Allyl Complex Supported by a Perchlorinated Carboranyl Phosphine. *Inorg. Chem.* **2015**, *54*, 5142–5144.

(35) Piche, L.; Daigle, J. C.; Rehse, G.; Claverie, J. P. Structure-activity Relationship of Palladium Phosphanesulfonates: Toward Highly Active Palladium-based Polymerization Catalysts. *Chem. Eur. J.* **2012**, *18*, 3277–3285.

(36) Britovsek, G. J. P.; Malinowski, R.; McGuinness, D. S.; Nobbs, J. D.; Tomov, A. K.; Wadsley, A. W.; Young, C. T. Ethylene Oligomerization Beyond Schulz–Flory Distributions. *ACS Catal.* **2015**, *5*, 6922–6925.

(37) Ittel, S. D.; Johnson, L. K.; Brookhart, M. Late-Metal Catalysts for Ethylene Homo- and Copolymerization. *Chem. Rev.* **2000**, *100*, 1169–1204.

(38) Seger, M. R.; Maciel, G. E. Quantitative 13C NMR Analysis of Sequence Distributions in Poly(ethylene-co-1-hexene). *Anal. Chem.* **2004**, *76*, 5734–5747.

(39) Wiedemann, T.; Voit, G.; Tchernook, A.; Roesle, P.; Göttker-Schnetmann, I.; Mecking, S. Monofunctional Hyperbranched Ethylene Oligomers. *J. Am. Chem. Soc.* **2014**, *136*, 2078–2085.

(40) Azoulay, J. D.; Bazan, G. C.; Galland, G. B. Microstructural Characterization of Poly(1-hexene) Obtained Using a Nickel α-Keto-β-diimine Initiator. *Macromolecules* **2010**, *43*, 2794–2800.

(41) Liu, W.; Rinaldi, P. L.; McIntosh, L. H.; Quirk, R. P. Poly(ethylene-*co*-1-octene) Characterization by High-Temperature

Multidimensional NMR at 750 MHz. *Macromolecules* **2001**, *34*, 4757–4767.

(42) Hansen, E. W.; Blom, R.; Bade, O. M. N.m.r. Characterization of Polyethylene with Emphasis on Internal Consistency of Peak Intensities and Estimation of Uncertainties in Derived Branch Distribution Numbers. *Polymer* **1997**, *38*, 4295–4304.

(43) Zhou, X.; Bontemps, S.; Jordan, R. F. Base-Free Phosphine−Sulfonate Nickel Benzyl Complexes. *Organometallics* **2008**, *27*, 4821–4824.

(44) Kolbert, A. C.; Didier, J. G.; Xu, L. Mechanochemical Degradation of Ethylene−propylene Copolymers: Characterization of Olefin Chain Ends. *Macromolecules* **1996**, *29*, 8591–8598.

(45) Prasad, A.; Mandelkern, L. Equilibrium Dissolution Temperature of Low Molecular Weight Polyethylene Fractions in Dilute Solution. *Macromolecules* **1989**, *22*, 914–920.

(46) Kanazawa, M.; Ito, S.; Nozaki, K. Ethylene Polymerization by Palladium/phosphine–sulfonate Catalysts in the Presence and Absence of Protic Solvents: Structural and Mechanistic Differences. *Organometallics* **2011**, *30*, 6049–6052.

(47) Anselment, T. M. J.; Wichmann, C.; Anderson, C. E.; Herdtweck, E.; Rieger, B. Structural Modification of Functionalized Phosphine Sulfonate-Based Palladium(II) Olefin Polymerization Catalysts. *Organometallics* **2011**, *30*, 6602–6611.

(48) Skupov, K. M.; Piche, L.; Claverie, J. P. Linear Polyethylene with Tunable Surface Properties by Catalytic Copolymerization of Ethylene with *n*-Vinyl-2-pyrrolidinone and *n*-Isopropylacrylamide. *Macromolecules* **2008**, *41*, 2309–2310.

(49) Reynhardt, E. C. Temperature Dependence of the Cell Parameters of Fischer-Tropsch Waxes: Hard Wax and Oxidised Hard Wax. *J. Phys. D, Appl. Phys.* **1986**, *19*, 1925–1938.

(50) Ciesińska, W.; Liszyńska, B.; Zieliński, J. Selected Thermal Properties of Polyethylene Waxes. *J Therm Anal Calorim* **2016**, *125*, 1439–1443.

(51) Hato, M. J.; Luyt, A. S. Thermal Fractionation and Properties of Different Polyethylene/wax Blends. *J. Appl. Polym. Sci.* **2007**, *104*, 2225–2236.

(52) Mpanza, H.; Luyt, A. Influence of Different Waxes on the Physical Properties of Linear Low-density Polyethylene. *S. Afr. J. Chem* **2006**, *59*, 48–54.

(53) Retief, J. J.; le Roux, J. H. Crystallographic Investigation of a Paraffinic Fischer-Tropsch Wax in Relation to a Theory of Wax Structure and Behaviour. *S. Afr. J. Sci.* **1983**, *79*, 234–239.

(54) Möller, M.; Cantow, H.; Drotloff, H.; Emeis, D.; Lee, K.; Wegner, G. Phase Transitions and Defect Structure in the Lamellar Surface of Polyethylene and *n*- alkane Crystallites. Magic Angle Spinning ^{13}C NMR Studies. *Die Makromolekulare Chemie* **1986**, *5*, 1237–1252.

(55) Luyt, A. S.; Krupa, I. Thermal Behaviour of Low and High Molecular Weight Paraffin Waxes Used for Designing Phase Change Materials. *Thermochim. Acta* **2008**, *467*, 117–120.

(56) Mandelkern, L.; Price, J. M.; Gopalan, M.; Fatou, J. G. Sizes and Interfacial Free Energies of Crystallites Formed from Fractionated Linear Polyethylene. *J. Polym. Sci. A-2 Polym. Phys.* **1966**, *4*, 385–400.

(57) Guo, X.; Pethica, B. A.; Huang, J. S.; Prud'homme, R. K. Crystallization of Long-Chain *n*-Paraffins from Solutions and Melts As Observed by Differential Scanning Calorimetry. *Macromolecules* **2004**, *37*, 5638–5645.

(58) Benn, R. Dynamic ^{1}H NMR Spectroscopy of η^2-ethylene Transition Metal Complexes. *Org. Magn. Reson.* **1983**, *21*, 723–726.

(59) The Pd-Me and the polymer chain methyl resonances are included in this calculation because they cannot be resolved from the the other Pd-R' resonances that are growing in. Assuming that the Pd-Me and Pd-R' species have similar insertion rate constants, only the y-intercept of the plots of X_n versus time are affected as the total number of of total methyl groups, from Pd-Me and the polymer chain methyls, is constant.

(60) Gu, W.; McCulloch, B. J.; Reibenspies, J. H.; Ozerov, O. V. Improved Methods for the Halogenation of the $[HCB_{11}H_{11}]^-$ Anion. *Chem. Commun.* **2010**, *46*, 2820–2822.

(61) Santos, L. S.; Metzger, J. O. On-line Monitoring of Brookhart Polymerization by Electrospray Ionization Mass Spectrometry. *Rapid Commun. Mass Spectrom.* **2008**, *22*, 898–904.

(62) The batch of **9** used for the low temperature experiments contained 15% of the corresponding CH_3CN complex.

(63) Grinshpun, V.; Rudin, A. Measurement of Mark- Houwink Constants by Size Exclusion Chromatography with a Low Angle Laser Light Scattering Detector. *Makromol. Chem., Rapid. Commun.* **1985**, *6*, 219–223.

Table of Contents Graphic